MUON ENERGY LOSS AT HIGH ENERGY AND IMPLICATIONS FOR DETECTOR DESIGN

J. J. Eastman and S. C. Loken

Lawrence Berkeley Laboratory

University of California, Berkeley, CA 94720

Abstract

We study the effects of energy loss and associated electromagnetic showers on muon tracking and momentum measurement in muon detectors operating in the energy range 100 GeV–5 TeV. A detailed Monte Carlo simulation tracks muons and shower particles through a detector structure and evaluates the charged-particle environment in chambers. We find that catastrophic energy loss events accompanied by energetic showers can pose serious problems to designers of muon spectrometers.

1 Introduction

In the energy regime to be explored by the SSC, traditional methods of muon identification and momentum measurement are complicated by the introduction of new energy loss mechanisms. At muon energies above a few hundred GeV, radiative processes dominate over ionization as sources of muon energy loss. These processes, bremsstrahlung and direct production of electron pairs, give rise to photons or electrons which can carry a significant fraction of the muon energy. In a muon spectrometer or calorimeter, the hard photons or electrons will initiate electromagnetic cascades which can obscure the muon track in active detector planes, making a precision position measurement in those planes impossible.

A number of groups have reviewed the mechanisms for energy loss by muons. This work has been done in connection with precision muon spectrometers for fixed target experiments [1,2,3] and in SSC studies [4]. The purpose of the study reported here is to investigate in detail the effects of showers on muon tracking. We have developed a Monte Carlo simulation that transports muons through material and models their energy loss and angular deflection arising from bremsstrahlung, direct e^+e^- pair production, ionization, multiple Coulomb scattering and photonuclear interactions. Bremsstrahlung photons and electron pairs are generated in discrete events along the muon path. The resulting electromagnetic showers are modeled

1

Figure 1: Contributions of several processes to the average energy loss of a muon in 5 m of iron as a function of muon energy. The processes are (p) direct e^+e^- pair production, (b) bremsstrahlung, (n) photonuclear interactions, and (i) ionization; t marks the total loss.
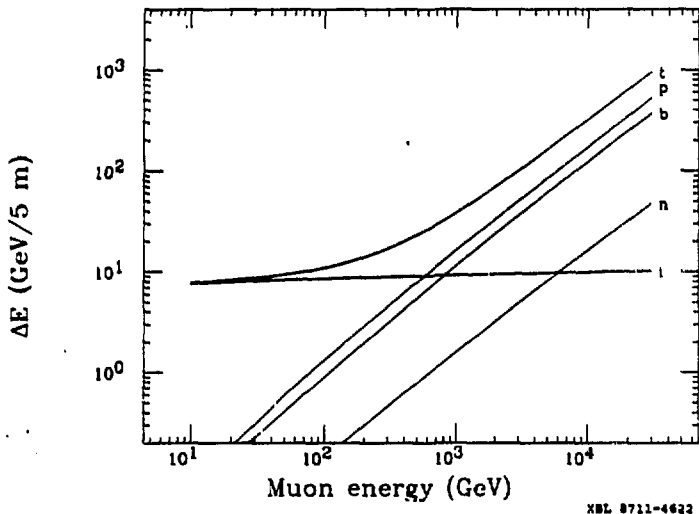
using the EGS4 Monte Carlo code [5] to determine occupancy rates and hit distributions in the active layers in two model detector configurations.

In the next section, we review the energy-loss processes and describe their parameterizations. We then discuss the behavior of hard electromagnetic showers in typical muon spectrometer configurations. Results are presented in Section 3 for muon energies from 100 GeV to 5 TeV.

2 Muon transport in matter

High energy muons passing through matter lose energy by ionization, bremsstrahlung, direct pair production, and photonuclear interactions. Our muon transport code simulates each of these processes. Figure 1 shows the average contribution of each process to the total average energy loss of a muon in 5 m of iron as a function of the muon energy.

In our treatment, ionization energy loss is considered to be continuous and uniform over the transport, and the hard processes, which occur relatively rarely in a meter of iron, are considered stochastically. These hard processes, characterized by sudden large energy losses and high-multiplicity showers, make muon tracking

2

and momentum reconstruction difficult.

2.1 Ionization

The dominant source of energy loss at muon energies below a few hundred GeV is ionization of the traversed medium. For thick detector elements, the Landau fluctuations in the ionization dE/dx can be safely ignored and the average used. Because of its large cross section, ionization is approximated in our Monte Carlo program as a continuous process. Each time the muon is transported, the step taken is broken into many smaller substeps. In each substep, the average ionization energy loss is subtracted from the muon energy.

The average ionization energy loss per unit length x (x in g/cm^2) is given by the Bethe-Bloch equation [6]:

$$\left(\frac{dE}{dx}\right)_{\text{Ion}} = 2\pi r_e^2 \frac{Z N_A}{A} \frac{m_e}{\beta^2} \left\{ \ln \frac{2m_e \beta^2 \gamma^2 E_m'}{I^2} - 2\beta^2 + \frac{1}{4}\frac{{E_m'}^2}{E_\mu^2} - \delta \right\}, \tag{1}$$

where E_m' is the largest kinematically allowed energy transfer to the electron:

$$E_m' = 2m_e \frac{p^2}{m_e^2 + m_\mu^2 + 2m_e E_\mu}, \tag{2}$$

r_e is the classical electron radius, N_A is Avogadro's number, Z and A are the atomic number and atomic weight of the medium, I is the medium's mean ionization potential, m_e and m_μ are the electron and muon masses, β and γ are the usual relativistic variables, and δ is the density effect correction. Sternheimer et al. [7] parameterize δ as a function of $X = \log_{10}(\beta\gamma)$ as

$$\delta = \begin{cases} 2X\ln 10 + a(X_1 - X)^m + C, & X_0 < X < X_1, \\ 2X\ln 10 + C, & X > X_1, \end{cases} \tag{3}$$

where X_0, X_1, a, m, and C are empirical material-dependant coefficients [8].

2.2 Stochastic processes

As it transports a muon, our Monte Carlo program determines when to generate a stochastic process by computing the total cross section for each of the processes simulated. The mean free path λ (in g/cm^2) is the inverse of the total cross section per gram. The muon is then transported a distance $-\lambda \ln(r)$, where r is a random number from 0 to 1, and the particular interaction to be simulated at the end of the transport is selected according to its contribution to the total cross section.

The energy fraction v lost by the muon in the interaction is drawn randomly from the distribution $\sigma^{-1} d\sigma/dv$. For each process, we use an unnormalized parameterization of the differential cross section derived by Van Ginneken [9] that is simple

3

enough in form to be integrated analytically to obtain the total cross section and inverted explicitly for drawing v. The parameterization is normalized by carrying out a more detailed calculation of the differential cross section at one value of v, and scaling the parameterized function to match the detailed calculation at that point. The average energy loss to each process, computed either by explicit integration of $E_\mu v d\sigma/dv$ or by recording discrete energy loss events in a large number of Monte Carlo runs, matches the tabulated values of ref. [6] at the 5% level for muon energies in the range 50 GeV–10 TeV.

Photons or e^+e^- pairs are generated with the selected energy fraction v and are passed to EGS for propagation through the detector structure. Shower particles are followed until their energies fall below 1.5 MeV.

In the expressions that follow, energies and masses are expressed in GeV.

2.2.1 Bremsstrahlung

The *total cross section* for muon bremsstrahlung is not large – the probability for a 1 TeV muon to bremsstrahlung in 1 m of iron is 5% – but the probability $v d\sigma/dv$ for producing a photon of energy $v E_\mu$ is nearly flat across a wide range of values of v. This means that bremsstrahlung contributes a tail of catastrophic loss to the muon energy loss distribution, and that the treatment of this process as a continuous contribution to the average energy loss is a very poor approximation.

The detailed calculation in this case is that of Petrukhin and Shestakov [10], who provide the following expression for the differential cross section for bremsstrahlung, taking into account the effects of nuclear and atomic form factors:

$$\left(\frac{d\sigma}{dv}\right)_{\text{Brem}} = \alpha\left(2Zr_e\frac{m_e}{m_\mu}\right)^2\left(\frac{4}{3} - \frac{4}{3}v + v^2\right)\frac{1}{v}\ln\frac{\frac{2}{3}A_R\frac{m_\mu}{m_e}Z^{-2/3}}{1 + \frac{A_R\sqrt{e}}{2}\frac{m_\mu^2}{m_e E_\mu}\frac{v}{1-v}Z^{-1/3}}, \quad (4)$$

for $Z > 10$. Here $e = 2.178\ldots$, and $A_R = 189$ is the radiation logarithm.

The parameterization of Van Ginneken of the differential cross section for muon bremsstrahlung from a nuclear target [1] is

$$\sigma^{-1}\frac{d\sigma}{dv} = \begin{cases} k_1 v^{-1}, & v_{\text{min}} < v < 0.03, \\ k_2 v^{-m}, & 0.03 < v < v_2, \\ k_3(1-v)^n, & v_2 < v < 1. \end{cases} \quad (5)$$

Here k_1, k_2, and k_3 are fixed by continuity and by the condition that the differential cross section must match Equation 4 at a specific point v_{norm} in the k_2 domain; $m = 1.39 - 0.024\ln E_\mu$; $n = 1.32 - 0.12\ln E_\mu$; $v_{\text{min}} = 0.001/E_\mu$; and $v_2 = \sqrt{E_\mu}/(\sqrt{E_\mu} + 4.5)$. The k_i depend in general on E_μ, Z and the normalization point v_{norm}, which itself varies with E_μ.

---

[1] We use Van Ginneken's parameterization for bremsstrahlung from nuclear targets, but normalize it as though it represented the differential cross section for all contributions to muon bremsstrahlung.

4

2.2.2 Direct pair production

At energies above ~ 500 GeV in iron, and ~ 150 GeV in uranium, direct e^+e^- pair production becomes the single most important source of muon energy loss. Unlike the bremsstrahlung case, the pair energy probability peaks at low energies, making high-energy pairs relatively unlikely.

For muon energies above ~ 100 GeV both e^+e^- and $\mu^+\mu^-$ pair production are possible. $\mu^+\mu^-$ production by muons is a potentially important process that can lead to misassignment of the sign of the incident muon, but this mechanism contributes less than 0.01% to the total energy loss [6] and is not modeled in the present study.

Kel'ner and Kotov [11] give the following expression for the differential cross section for e^+e^- production by muons, which includes form factors:

$$\left(\frac{d\sigma}{dv}\right)_{\text{Pair}} = \frac{16}{v\pi}(Z\alpha r_e)^2[F_a(E_\mu, v) + F_b(E_\mu, v)], \tag{6}$$

with

$$
\begin{aligned}
F_a(E_\mu, v) &= \int_{1/E_\mu v}^{1/2} dx_+ \int_{t_{\min}}^{\infty} \frac{dt}{t^2} \left\{ \left[t\left(1 - v + \frac{v^2}{2}\right) - m_\mu^2 v^2 \right] \right. \tag{7} \\
&\quad \times \left[\frac{1}{\gamma}\left(\frac{1}{2} - x_+ x_-\right) + \frac{x_+ x_-}{6\gamma^2}(2 - t) \right] \\
&\quad + \left. \frac{t x_+^2 x_-^2}{3\gamma^2}\left[t\left(3(1 - v) + \frac{v^2}{2}\right) - m_\mu^2 v^2 \right] \right\} \ln \frac{A_R Z^{-1/3}\sqrt{\gamma}}{\zeta b + 1}, \\
F_b(E_\mu, v) &= \frac{1}{12m_\mu^2}\left[\left(\frac{4}{3} - \frac{4}{3}v + v^2\right)\left(\ln \frac{m_\mu^2 v^2}{1 - v} - \frac{5}{3}\right) + 1 - \frac{1}{3}(1 + v)^2 \right] \\
&\quad \times \ln \left[\frac{A_R m_\mu Z^{-1/3}}{\frac{A_R \sqrt{e}}{2} Z^{-1/3} \frac{m_\mu v^2}{E_\mu(1 - v)} + 1} \right],
\end{aligned}
$$

where $x_\pm$ are the fractions of the pair energy $\omega = vE_\mu$ carried by the positron and electron, $-t$ is the square of the four-momentum transferred to the muon, $\gamma = 1 + tx_+ x_-$, $\zeta = 100\gamma Z^{-1/3}/\omega x_+ x_-$, $b = A_R\sqrt{e}/200$, and $t_{\min} = m_\mu^2 v^2/(1 - v)$. In practice the computationally expensive double integral was evaluated numerically at a number of points to form a lookup table; the value of the differential cross section at a given E_μ, v, and Z was found by interpolation as needed.

Van Ginneken provides the following approximation to the differential cross section:

$$
\sigma^{-1}\frac{d\sigma}{dv} = \begin{cases} k_0, & 5m_e/E_\mu < v < 25m_e/E_\mu, \\ k_1 v^{-1}, & 25m_e/E_\mu < v < .002, \\ k_2 v^{-2}, & .002 < v < .02, \\ k_3 v^{-3}, & .02 < v < 1. \end{cases} \tag{8}
$$

5

k_0, k_1, k_2 and k_3 are fixed by continuity and by requiring that the differential cross section match Eq. 6 at a point in the k_2 region, which is the region responsible for the bulk of the energy loss.

2.2.3 Photonuclear interactions

Photonuclear interactions account for about 5% of the total energy loss of high-energy muons in iron, and about 2% in uranium. The losses are concentrated in rare, relatively hard events. In this paper we consider these interactions as a contribution to the energy loss but we do not simulate hadronic showers.

Bezrukov and Bugaev [12] present the following expression for the differential cross section for photonuclear interactions of muons, including a correction for nucleon shadowing effects:

$$
\left(\frac{d\sigma}{dv}\right)_{\mu A} = \frac{\alpha}{2\pi} A\sigma_{\gamma N}(vE_\mu)v\left\{0.75G(x)\left[\kappa\ln\left(1+\frac{m_1^2}{t}\right)-\frac{\kappa m_1^2}{m_1^2+t}-\frac{2m_\mu^2}{t}\right]\right.
$$
$$
+ 0.25\left[\kappa\ln\left(1+\frac{m_2^2}{t}\right)-\frac{2m_\mu^2}{t}\right]
$$
$$
\left.+\frac{m_\mu^2}{2t}\left[0.75G(x)\frac{m_1^2}{m_1^2+t}+0.25\frac{m_2^2}{t}\ln\left(1+\frac{t}{m_2^2}\right)\right]\right\},
$$

(9)

where $t = m_\mu^2 v^2/(1-v)$, $\kappa = 1-2/v+2/v^2$, $m_1^2 = 0.54$ GeV^2, $m_2^2 = 1.8$ GeV^2, $\sigma_{\gamma N}(E) \simeq 114.3 + 1.647\ln^2(0.0213E)$ μb is the total photoabsorption cross section on nucleons, $x = 0.00282A^{1/3}\sigma_{\gamma N}(E_\mu v)$, and $G(x) = (3/x^3)(x^2/2-1+e^{-x}(1+x))$.

Van Ginneken's parameterization is based not on this expression but on a simpler treatment that uses leptoproduction scaling and parameterizations of measured structure functions. The formula is

$$
\sigma^{-1}\frac{d\sigma}{dv} = \begin{cases} k_1(E_\mu v)^2, & 0.144 < E_\mu v < 0.35, \\ k_2(E_\mu v)^{-1.11}(1-v)^2, & 0.35 < E_\mu v < E_\mu - m_\mu. \end{cases}
$$

(10)

As before k_1 and k_2 are fixed by continuity and by matching the parameterized differential cross section to Equation 9 at a value of v in the k_2 domain.

3 Implications for detectors

Figure 2 illustrates a model spectrometer used in this study. The spectrometer is a stack of five unmagnetized iron blocks 1 meter thick. Chambers between the blocks are used to measure the muon position. Electromagnetic interactions in the iron produce showers that can penetrate the chambers. The 1-meter blocks are sufficiently thick to eliminate correlations in shower hits among the chambers.

Figure 2: A 1 TeV muon traverses a model detector used in the study. Five thin chambers alternate with five 1-meter slabs of iron. The muon (entering from the right) has undergone four substantial pair-production events and a number of smaller interactions in the iron. All charged particle paths are shown.
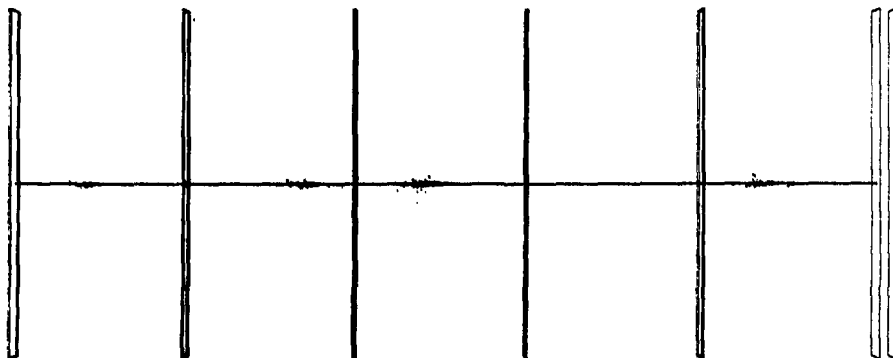
A second detector configuration used in limited-statistics runs was a 90 cm uranium slab followed by a single chamber. This configuration was used to study the charged particle environment at the exit of a hadron calorimeter.

3.1   Energy loss

Figure 3 shows various contributions to the energy loss spectrum per muon for 10000 1 TeV muons traversing 5 m of iron. The total energy lost in the 5 m by each muon to each hard process is histogrammed. The striking features of these distributions are the long tails associated with catastrophic energy losses.

Because of energy loss in the material of a muon spectrometer, the muon momentum measured in the spectrometer will be significantly less than the incident momentum. The measured momentum can be corrected on average and the fluctuations in energy loss are comparable to the typical resolution of a solid iron muon spectrometer. The fluctuations in energy loss are, however, significantly greater than the precision of an air-gap spectrometer. If the muon momentum is to be determined outside a thick calorimeter, as in the L3+1 proposal [13], it is necessary to reconstruct the lost energy for each event to achieve the full detector resolution.

3.2 Chamber illumination

The most significant result of the energy loss processes is the electromagnetic showers that are initiated by the photons and electron pairs. For a 1 TeV muon, the typical shower energy is of order 100 GeV and the shower will develop over approximately 50 cm of the muon track. Any detector plane in a muon spectrometer has a significant probability of being near the maximum of an electromagnetic shower. We assume that any detector plane containing more than one charged track will be rejected in reconstructing the muon trajectory as it is impossible to isolate the muon hit among the shower particles. Substantial tracking inefficiencies can result in geometries where all chambers are needed to perform a reasonable momentum measurement.

Figure 4 (a) is the histogram of hit frequency per plane per event for active planes in the detector of Figure 2 for 1 TeV muons. The probability of having more than one charged particle track in a given plane is $20.2 \pm 0.4\%$ (statistical error only). Figure 4 (b) shows the hit frequency in an active plane placed after a 90-cm slab of uranium in a limited statistics run at 1 TeV. In this case the multiple-hit probability is $26\pm3\%$. This shows that a muon plane placed at the exit of a uranium calorimeter can suffer serious inefficiencies.

The single-hit probability is shown in Figure 5 as it falls with increasing muon energy. At 1 TeV in iron, if three out of three chambers are required for a momentum measurement, the probability of finding a measurable track is only 51%. Clearly this sort of geometry is to be avoided. If three out of four chambers are required, the probability of a measurable track rises to 82%; a substantial inefficiency remains.

3.3 Multi-hit requirements for chambers

Some SSC muon detector designs [13,14] have featured muon position resolutions in the barrel region of on the order of 100 μ. If, however, the detector's two-track resolution is too large, planes containing multiple hits may not be tagged as such. In this case the muon position measurement is smeared by the size of the shower, which is typically much larger than the nominal resolution. It is therefore important that a detector be able to tag such multiply-hit planes and remove them from the momentum fit. We have used our simulation to examine the requirements for reasonable tagging.

In our model, an active detector plane is characterized by a two-track resolution σ_{2T}. We assume that a detector plane can be tagged as multiply hit by some means (eg. pulse width or height analysis) if the plane contains more than 20 hits. Otherwise, we tag a multiply hit plane only if it contains at least one pair of hits separated by more than σ_{2T}. Figure 6 shows the efficiency for tagging a multiply-hit detector plane by this method as a function of σ_{2T}. The residual $\sim 10\%$ efficiency at very large σ_{2T} comes from the 20-hit tagging capability. The tagging efficiency drops

Figure 3: Energy loss per muon from each of several processes for 10000 1 TeV muons in the detector of Figure 2. Shown are the contributions from a) bremsstrahlung; b) direct e^+e^- pair production; and c) deep inelastic scattering on nucleons. Note the substantial tails.
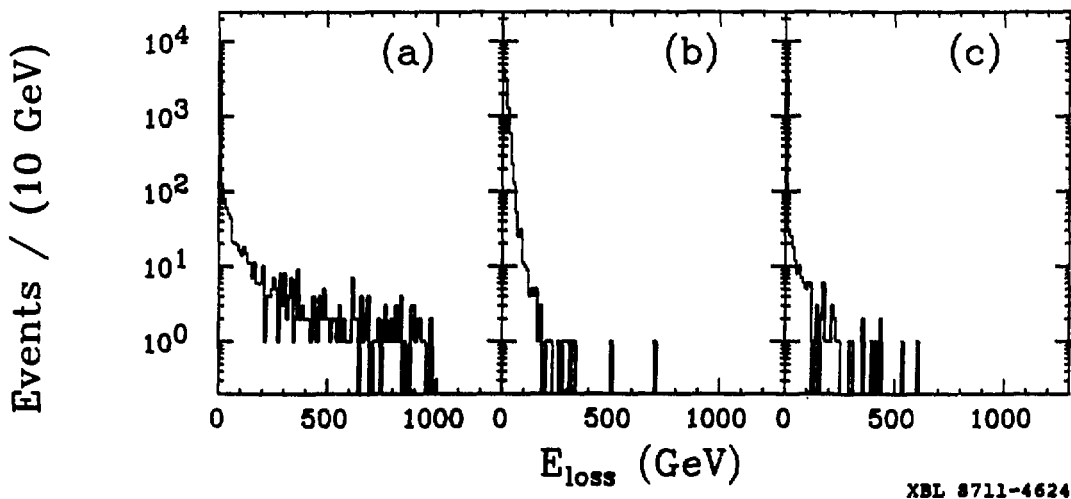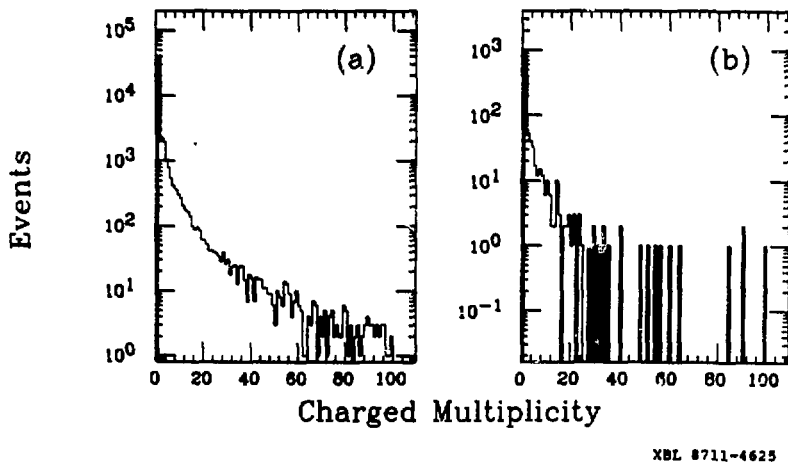
Figure 4: a) The hit multiplicity for 1 TeV muons in the active planes of the detector of Figure 2 and b) in an active plane after 20 cm of uranium.

dramatically for σ_{2T} greater than about 1 mm. Obtaining two-track resolutions of this size in large chambers is a challenge for detector designers.

4   Conclusions

Muon energy loss will have a significant impact on detector design for the SSC. Localized energy loss events can make momentum reconstruction more difficult. Electromagnetic showers in detector materials will obscure muon tracks in many planes of the detector and will reduce the tracking efficiency at high energy. Unresolved shower particles can also worsen position measurements. Muon spectrometer designs could incorporate open geometries, shower energy reconstruction, multiple redundancy cf measurement, and multi-hit capabilities to combat these problems.

Figure 5: The probability of a clean muon hit (i.e., a muon track unaccompanied by any other charged particle) in an active layer in the detector of Figure 2 as a function of E_μ (diamonds). Also included are two points for an active layer placed behind 90 cm of uranium (crosses).
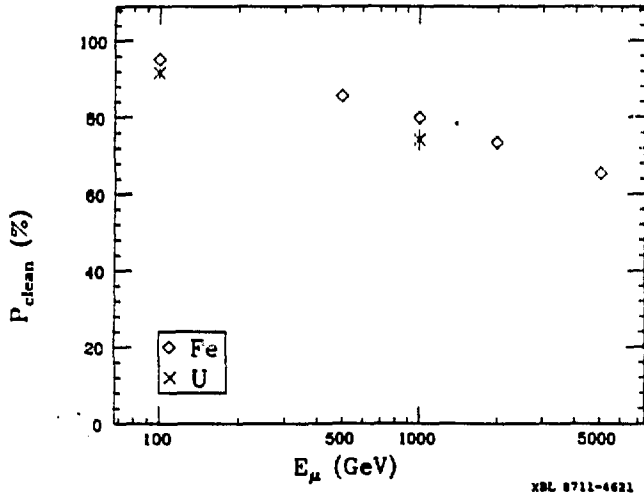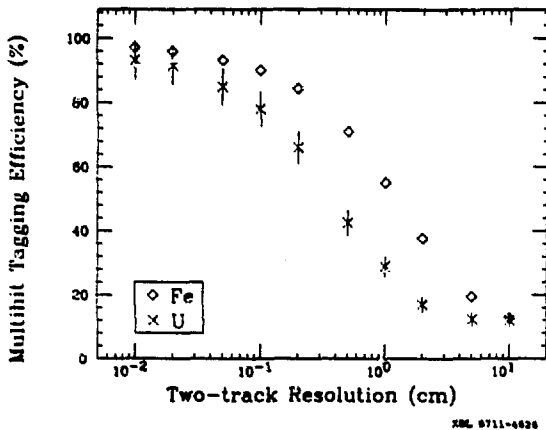

Figure 6: The probability of identifying a multiply hit chamber as a function of the chamber's two-track resolution for active planes in the detector of Figure 2 and for an active layer placed behind 90 cm of uranium. Assumptions are given in the text.

References

[1] R. Kopp *et al.* (the BCDMS Collaboration). *Z. Phys.* *C* **28**, 171 (1985).

[2] F.C. Shoemaker. *Bremsstrahlung by muons in iron.* Kerth Group Internal Note GIN-153, Lawrence Berkeley Laboratory, 1980.

[3] F.C. Shoemaker. *Direct pair production by muons in iron.* Kerth Group Internal Note GIN-155, Lawrence Berkeley Laboratory, 1980.

[4] Muon Detector Subgroup. SSC muon detector group report. In R. Donaldson and J. Marx, editors, *Physics of the Superconducting Supercollider: Snowmass 1986*, page 405, 1986.

[5] W.R. Nelson, H. Hirayama and D.W.O. Rogers. *The EGS4 Code System.* SLAC Report SLAC-265, Stanford Linear Accelerator Center, 1985.

[6] W. Lohmann, R. Kopp and R. Voss. *Energy Loss of Muons in the Energy Range 1-10000 GeV.* CERN Report CERN 85-03, European Organization for Nuclear Research, 1985.

[7] R.M. Sternheimer. *Phys. Rev.* **103**, 511 (1956).

[8] R.M. Sternheimer, S.M. Seltzer and M.J. Berger. *Atomic Data & Nucl. Data Tables* **30**, 261 (1984).

[9] A. Van Ginneken. *Nucl. Instr. Meth.* **A251**, 21 (1986).

[10] A.A. Petrukhin and V.V. Shestakov. *Can. J. Phys.* **46**, S377 (1968).

[11] S.R. Kel'ner and Yu.D. Kotov. *Sov. J. Nucl. Phys.* **7**, 237 (1968).

[12] L.B. Bezrukov and É.V. Bugaev. *Sov. J. Nucl. Phys.* **33**, 635 (1981).

[13] U. Becker *et al.* *Nucl. Inst. Meth.* **A253**, 15 (1986). Also see submission to these proceedings.

[14] R. Thun, C.-P. Yuan *et al.* *Searching for Higgs $\to Z^0 Z^0 \to \mu^+\mu^-\mu^+\mu^-$ at SSC.* Physics Department Report UM HE 86-32, University of Michigan, 1986. Also see submission to these proceedings.